Theory of inelastic x-ray scattering by phonons in ice

Peter Johansson
European Synchrotron Radiation Facility, Boîte Postale 220, F–38043 Grenoble, France
(Received 25 March 1996)

We calculate the inelastic x-ray scattering phonon line shape in ice. The interaction between molecules is described by the simple point charge potential, averaged over different relative orientations of the molecules. We investigate different mechanisms that can broaden the phonon lines. We find that bond disorder only gives a small contribution to the linewidth. Anharmonicity, on the other hand, gives significant broadening of the phonon peak, and the variation of the width as a function of momentum transfer is in qualitative agreement with experiment. [S0163-1829(96)06729-X]

In a recent series of experiments Sette, Ruocco, and coworkers measured the dynamic structure factor in water and in ordinary ice (ice Ih) by means of inelastic x-ray scattering (IXS) with very high energy resolution.[1,2] This technique has some clear advantages over inelastic neutron scattering[3,4] (INS) in the study of these systems. IXS is not subject to the same kinematic constraints as INS. Therefore one gets access to a larger domain of momentum transfer-energy $(\mathbf{q},\omega)$ space, the dynamic structure factor can be measured in a more direct way, and maybe most importantly, results from the liquid and the solid can be compared directly. The most striking experimental findings are the following:[1,2] (i) The speed of sound in water and in ice is nearly the same when $|\mathbf{q}|\gtrsim 3\ \mathrm{nm}^{-1}$. This speed is typically twice that of long-wavelength hydrodynamic sound in water. (ii) This fast-sound propagation involves center-of-mass motion of the molecules in the liquid. (iii) There is an almost steplike increase of the phonon peak width at $|\mathbf{q}|\approx 7$–$8\ \mathrm{nm}^{-1}$ by about 6–7 meV [full width at half maximum (FWHM)], in both ice and water. (iv) In the ice spectra, an extra peak shows up at low energy for $|\mathbf{q}|\gtrsim 10\ \mathrm{nm}^{-1}$.

In the following, we calculate inelastic x-ray scattering spectra for ice by employing a simple model for the molecule-molecule interaction. The main objective is to attempt an explanation of the broadening of the phonon peaks. To this end we study the effects of anharmonicity and the disorder that is inherently present in ice. Anharmonicity is important because the molecule-molecule interaction is the sum of two different contributions: a Lennard-Jones (LJ) term which is strongly repulsive at the equilibrium intermolecular distance and an attractive electrostatic interaction. The resulting potential is rather asymmetric with respect to the equilibrium configuration, and hence anharmonic. The disordered variations in the electrostatic interaction result from the fact that the H atoms can be oriented in different ways around an O atom.

We find that anharmonicity typically gives an appreciable broadening of the phonon peak for $|\mathbf{q}|\sim 8\ \mathrm{nm}^{-1}$ or larger. At these $\mathbf{q}$ one starts to excite phonons that are sensitive to the anharmonic part of the interaction. Thus the trend is the same as in the experiments, but the increase in width is more abrupt there. The effects of disorder are in contrast less important.

The inelastic x-ray scattering rate per unit energy and solid angle is related to the molecular density-density correlation function

$$\frac{dP}{d(\hbar\omega)d\Omega}=\frac{1}{\mathcal{A}}\frac{r_0^2}{2}|\boldsymbol{\epsilon}_f\cdot\boldsymbol{\epsilon}_i|^2|f(\mathbf{q})|^2 \times\int_{-\infty}^{\infty}\frac{dt}{2\pi\hbar}\langle\,\rho(\mathbf{q},t)\,\rho(-\mathbf{q},0)\rangle e^{i\omega t}. \quad (1)$$

Here r_0 is the Thomson radius, and $\boldsymbol{\epsilon}_i$ and $\boldsymbol{\epsilon}_f$ are the polarization vectors of the incident and outgoing photons, respectively. The molecular form factor is denoted $f(\mathbf{q})$, and $\mathcal{A}$ is the sample area. Since the average recoil energy $\hbar^2q^2/2M$ is of the order 0.1 meV while the typical phonon energy is of order 10 meV, it suffices to consider one-phonon processes. This yields

$$\frac{dP}{d(\hbar\omega)d\Omega}=\frac{\rho_M L}{32\pi M^2}r_0^2|\boldsymbol{\epsilon}_f\cdot\boldsymbol{\epsilon}_i|^2|f(\mathbf{q})|^2e^{-2W}[1+n(\omega)] \times\Big[-\mathrm{Im}\sum_{\lambda\lambda'}g_{\lambda\lambda'}(\mathbf{q}) \times[G^R_{\mathbf{q}\lambda\lambda'}(\omega)-G^A_{\mathbf{q}\lambda\lambda'}(\omega)]\Big], \quad (2)$$

where ρ_M is the mass density, L the sample thickness, M the molecule mass, e^{-2W} a Debye-Waller factor, and $n(\omega)$ a Bose occupation number. The sum runs over the phonon modes. The coupling factor $g_{\lambda\lambda'}$ depends on the phonon eigenvectors $\boldsymbol{\epsilon}_{\lambda\alpha\mathbf{q}_0}$,

$$g_{\lambda\lambda'}(\mathbf{q})=\sum_{\alpha\beta}e^{-i\mathbf{G}\cdot(\mathbf{R}_{0\alpha}-\mathbf{R}_{0\beta})}(\mathbf{q}\cdot\boldsymbol{\epsilon}^*_{\lambda\alpha\,\mathbf{q}_0})(\mathbf{q}\cdot\boldsymbol{\epsilon}_{\lambda'\beta\,\mathbf{q}_0}). \quad (3)$$

Here α and β denote the degrees of freedom of the molecules in the unit cell, $\mathbf{q}_0$ lies in the first Brillouin zone, $\mathbf{G}$ is a reciprocal lattice vector, and $\mathbf{q}=\mathbf{q}_0+\mathbf{G}$. The retarded and advanced phonon Green's functions are found from the Dyson equation

$$G_{\mathbf{q}\lambda\lambda'}=G^{(0)}_{\mathbf{q}\lambda\lambda'}+\sum_{\lambda_1\lambda_2}G^{(0)}_{\mathbf{q}\lambda\lambda_1}\Sigma_{\lambda_1\lambda_2}(\mathbf{q})G_{\mathbf{q}\lambda_2\lambda'}. \quad (4)$$

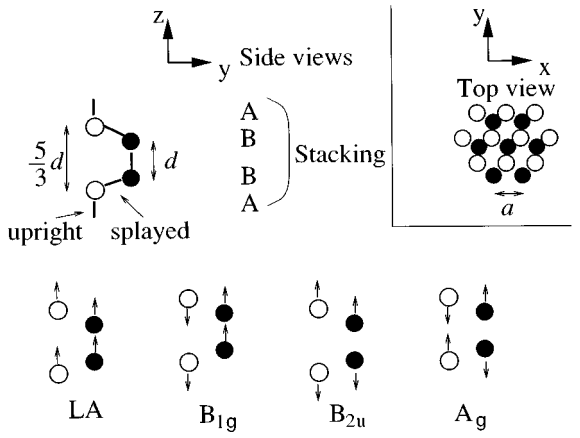

FIG. 1. Structure and simple vibrations of hexagonal ice. The O atoms occupy the sites of a wurtzite structure (hexagonal xy planes stacked in order ... ABBA ...). The distance between O atoms is $d=2.77$ Å and $a=\sqrt{8/3}d=4.52$ Å. The eigenvectors, at the zone center, of the nondegenerate vibrations (longitudinal in the z direction) are shown. Their dynamics and frequencies (see Fig. 2) can be understood in terms of strong (upright bonds) and weak (splayed bonds) springs connecting the different planes.

The bare Green's function for undamped phonons is

$$G^{(0)R,A}_{\mathbf{q}\lambda\lambda'}=2\delta_{\lambda\lambda'}[(\omega\pm i\delta)^2-\omega^2_{\mathbf{q}\lambda}]^{-1}.$$

The self-energy $\Sigma_{\lambda\lambda'}$ takes into account scattering processes due to disorder and anharmonicity (see below).

The structure of ordinary ice (ice Ih) is illustrated schematically in Fig. 1.[5,6] The O atoms occupy the lattice sites of a wurtzite structure. Each O atom has four nearest-neighbor oxygens situated 2.77 Å away at the corners of a tetrahedron. Between each pair of oxygens there is *one* H atom at a distance 1 Å from one of them, and each O has two H's next to it, but apart from this the exact arrangement of the H atoms is arbitrary.

We calculate the phonon frequencies and eigenvectors using the simple point charge (SPC) intermolecular potential.[7] It is a sum of Coulomb potentials acting between effective charges at the O and H atoms of *different* molecules, and a LJ potential acting between the O atoms,

$$V_{\mathrm{SPC}}=\frac{e^2}{4\pi\epsilon_0}\sum_{ij}\frac{q_iq_j}{r_{ij}}+4E_{\mathrm{LJ}}\left[\left(\frac{\sigma}{r_{\mathrm{OO}}}\right)^{12}-\left(\frac{\sigma}{r_{\mathrm{OO}}}\right)^{6}\right]. \quad (5)$$

The parameter values are $q_{\mathrm{H}}=0.41$, $q_{\mathrm{O}}=-0.82$, $E_{\mathrm{LJ}}=6.74$ meV, and $\sigma=3.17$ Å. Thus, the LJ radius σ is considerably larger than the O-O distance; in equilibrium there is a balance between the repulsive LJ interaction and the effectively attractive electrostatic interaction. We only include the completely dominating nearest-neighbor interactions, and average V_{SPC} over the different possible orientations of a molecule. At the same time we neglect molecular rotations, which is reasonable because the hindered rotation frequencies lie above the range of immediate interest. Furthermore, rotational motion couples very weakly to x rays.

The resulting dispersion relations along the y and z axes are shown in Fig. 2. In general, the calculation overestimates somewhat the phonon frequencies compared with experiment and calculations designed to fit the dispersion relations to experiment.[2,4,8–10] However, the frequencies decrease to some extent when anharmonicity is taken into account; moreover, the present study aims at finding trends rather than exact numbers so that the agreement is satisfactory.

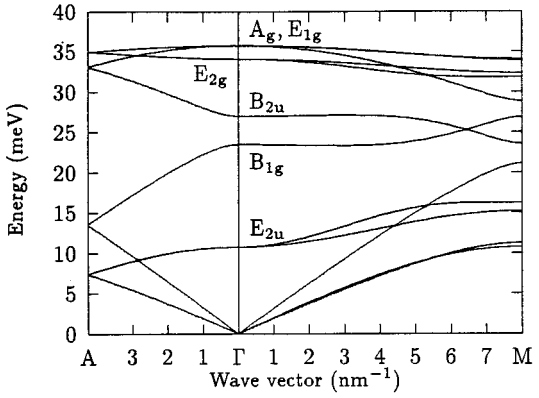

FIG. 2. Phonon dispersion relations in the y (ΓM) and z (ΓA) directions, respectively. The symmetry of the vibrations at the zone center is indicated; cf. Fig. 1 and Ref. 8.

The thin curves in Figs. 3 and 4 show calculated IXS spectra for a *harmonic* crystal. At long wavelengths the dominant peak in the spectrum comes from the LA mode. In this case $\mathbf{q}=\mathbf{q}_0$ and the coupling $g_{\lambda\lambda'}$ is significant only for modes where the molecules in the same unit cell move in phase. With increasing momentum transfer, shorter-wavelength phonons are excited. However, in certain directions and for large enough $|\mathbf{q}|$, it becomes again possible to excite the LA phonon. For a simple illustration take $\mathbf{q}\approx 2G\hat{z}$, where $G=3\pi/4d$. The contributions from the four molecules in the unit cell (cf. Fig. 1) add up constructively in Eq. (3), resulting in a sharp peak at low energy. This phe-

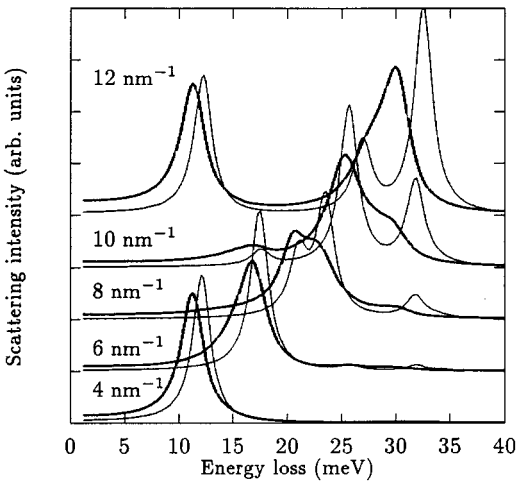

FIG. 3. Inelastic x-ray scattering probability as a function of energy loss with $\mathbf{q}$, given next to the curves, in the y direction. The thin curves were calculated within the harmonic approximation. A phenomenological peak width of 2 meV ($2\hbar\delta$) accounts for the experimental resolution. The thick curves show the results of calculations including effects of anharmonicity and disorder. The temperature was 250 K.

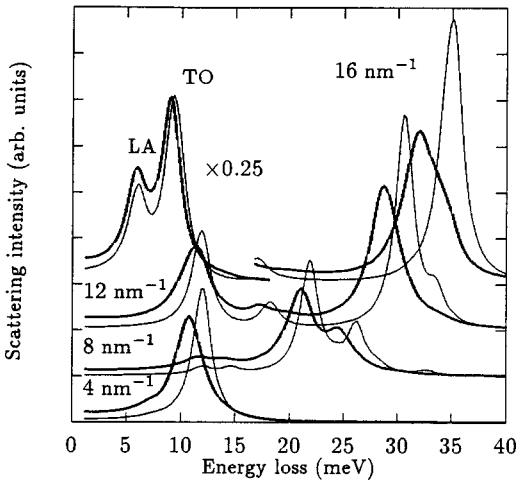

FIG. 4. Same as Fig. 3, but with $\mathbf{q}$ in the yz plane making a 20° angle with the y axis. The left part of the spectrum for $|\mathbf{q}|=16\ \mathrm{nm}^{-1}$ has been multiplied by 0.25.

nomenon shows up for $|\mathbf{q}|=12\ \mathrm{nm}^{-1}$ in Fig. 3. In directions of lower symmetry transverse optical (TO) phonons can also be excited when $\mathbf{q}$ lies outside the first Brillouin zone, and is aligned with the eigenvector $\epsilon_{\lambda\alpha\mathbf{q}_0}$ ($\mathbf{q}_0=\mathbf{q}-\mathbf{G}$). This yields the extra peak in the experimental spectra at $\hbar\omega\sim 7$–8 meV.[2,11] In Fig. 4 low-frequency peaks due to both LA and TO modes occur for $q=16\ \mathrm{nm}^{-1}$.

We begin the discussion of broadening mechanisms by looking at the bond disorder inherently present in ice. This leads to variations in the electrostatic interaction between different pairs of molecules depending on their relative orientation. In a certain configuration, there are consequently interactions that mix the phonon modes calculated with an orientation-averaged potential. We take these effects into account by evaluating the disorder contribution to the phonon self-energy within the Born approximation. This yields

$$\Sigma^{R,A}_{\lambda\lambda'}(\mathbf{q},\omega_0)=\frac{n_c^{-1}}{4M^2V_{\mathrm{BZ}}}\sum_{c,\lambda_1}\int d^3q_1 W^c_{\lambda\lambda_1}(\mathbf{q},\mathbf{q}_1)\times W^{c*}_{\lambda'\lambda_1}(\mathbf{q},\mathbf{q}_1)G^{(0)R,A}_{\mathbf{q}_1\lambda_1}(\omega_0), \tag{6}$$

where n_c is the number of configurations and the matrix elements $W^c_{\lambda\lambda_1}(\mathbf{q},\mathbf{q}_1)$ depend on the change in the dynamical matrix when the average charge configuration of two molecules is replaced by a real one labeled by c. The FWHM broadening of a phonon peak, $-2\mathrm{Im}\Sigma^R_{\lambda\lambda}/\omega_\lambda$, is typically less than 0.5 meV;[12] in some cases, for large $|\mathbf{q}|$, it is somewhat larger. Anyway, disorder alone cannot explain the behavior of the linewidth found experimentally. This result should be rather robust to details in the model potential because the strength of the disorder is in the end a function of the dipole moment of the H_2O molecule, which is fairly well known.

Consider now the more important effects of anharmonicity. Expanding the potential energy of the crystal to third order, and evaluating the corresponding lowest-order contribution to the phonon self-energy yields[13,14]

$$\Sigma^{R,A}_{\lambda\lambda'}(\mathbf{q},\omega_0)=\frac{\hbar}{16M^3}\frac{1}{V_{\mathrm{BZ}}}\sum_{\lambda_1\lambda_2}\int d^3q' V_{\lambda\lambda_1\lambda_2}(-\mathbf{q},\mathbf{q}',\mathbf{q}-\mathbf{q}')V_{\lambda'\lambda_1\lambda_2}(\mathbf{q},-\mathbf{q}',\mathbf{q}'-\mathbf{q})\frac{1}{\omega_1\omega_2}\times\left[\frac{1+n(\omega_1)+n(\omega_2)}{\omega_0\pm 2i\delta-\omega_1-\omega_2}-\frac{n(\omega_1)-n(\omega_2)}{\omega_0\pm 2i\delta-\omega_1+\omega_2}+[(\omega_0\pm 2i\delta)\rightarrow-(\omega_0\pm 2i\delta)]\right], \tag{7}$$

where

$$V_{\lambda\lambda'\lambda''}(\mathbf{q}_1,\mathbf{q}_2,\mathbf{q}_3)=\frac{1}{N}\sum_{ij\ell\alpha\beta\gamma}\frac{\partial^3V_{\mathrm{tot}}}{\partial u_{\alpha i}\partial u_{\beta j}\partial u_{\gamma\ell}}\epsilon^*_{\alpha\lambda}(\mathbf{q}_1)\epsilon^*_{\beta\lambda'}(\mathbf{q}_2)\epsilon^*_{\gamma\lambda''}(\mathbf{q}_3)e^{-i(\mathbf{q}_1\cdot\mathbf{R}_{i\alpha}+\mathbf{q}_2\cdot\mathbf{R}_{j\beta}+\mathbf{q}_3\cdot\mathbf{R}_{\ell\gamma})}. \tag{8}$$

Here $\omega_1=\omega_{\mathbf{q}'\lambda_1}$, $\omega_2=\omega_{\mathbf{q}-\mathbf{q}'\lambda_2}$, i, j, and ℓ run over the N unit cells of the crystal, and V_{tot} is the total potential energy. In the calculations we set the phenomenological damping $\hbar\delta=1$ meV. The different terms of Eq. (7) describe decay of a phonon into two, collision of a phonon with a thermally excited one, and events in which two thermally excited phonons merge into one. The latter type of process is important for anti-Stokes scattering in which the x ray gains energy. Since the combination of Eqs. (7) and (4) only gives a perturbative result, it is useful to have a check, such as the f-sum rule,[13] on the results. In general it is satisfied to within 7–8 % in our calculations. Finally, one should keep in mind that the above self-energy is rather sensitive to details in the interaction potential as it involves third derivatives.

Figures 3 and 4 show calculated results; for comparison we display results with and without effects of anharmonicity and disorder. In Table I we list experimental and theoretical FWHM linewidths. For small $|\mathbf{q}|$, the major effect of the anharmonicity is to shift the resonance towards lower energy by about 1 meV; the linewidth is almost unchanged. Once $\mathbf{q}$ lies in the next Brillouin zone, the phonon peaks are broader, and the extra width caused by anharmonicity is typically 2–3 meV. The calculated widths vary more with the direction than the experimental ones; for example, with $\mathbf{q}$ close to the z direction they are of the same size as in the experiment, but then perturbation theory is also about to break down. The only feature that is significantly affected by disorder is the high-frequency peak for 16 nm^{-1} in Fig. 4, where the disorder and anharmonicity contributions to the width are of similar strength.

TABLE I. Experimental and theoretical linewidths. The experimental values correspond to the Lorentzian fits made to the phonon peak (in single-crystal samples) in Ref. 2. The resolution, ≈ 3 meV, has been subtracted. To get a relatively unambiguous theoretical width we use the anharmonicity contribution to $-2\mathrm{Im}\Sigma^R_{\lambda\lambda}/\omega_\lambda$ calculated at the peak frequency for the mode with the largest $g_{\lambda\lambda}$. The peaks in the figures are wider because of the phenomenological broadening and sometimes two modes with almost equal frequencies are excited.

$\lvert\mathbf{q}\rvert$ (nm^{-1})	4	6	8	10	12
Experiment	0.5	1	8	7	9
Theory ($\mathbf{q}$ as in Fig. 3)	0.25	0.71	3.3	4.2	1.9
Theory ($\mathbf{q}$ as in Fig. 4)	0.27	0.66	1.5	1.6	2.6

The basic reason for the increase of the calculated linewidths is that optical phonons are more anharmonic than acoustic ones. The restoring force that gives an acoustic phonon is usually the sum of contributions from several weak springs (i.e., splayed bonds). In this case anharmonic effects do not play an important role. For an optical phonon, most of the restoring force instead typically comes from one strong spring. Thus considering a wave vector near the zone edge, the restoring forces and frequencies of acoustic and optical phonons may be nearly equal, yet the optical mode is much more affected by anharmonicity since it involves *relative motion* of molecules *parallel to the bond axis*. Consequently the phonon peak broadens considerably over a narrow range of momentum transfers near the Brillouin zone edge.

Comparing experiment and theory, we see that the linewidths differ in absolute numbers, but have one very important feature in common, namely, the marked increase at $\lvert\mathbf{q}\rvert \approx 8\ \mathrm{nm}^{-1}$. We think that this qualitative result is sufficiently independent of details in the potential that we can conclude that anharmonicity plays an important role as a broadening mechanism. Nevertheless, the large experimental linewidths suggest that some other mechanism may be important as well. Since the broadening due to anharmonicity varies approximately linearly with temperature, measurements at lower temperatures could clarify the situation considerably.

In summary, we have presented a theoretical study of mechanisms that can broaden the phonon peaks in inelastic x-ray scattering spectra of ice. The results show that the intrinsic disorder present in ice does not play a primary role. Anharmonicity, on the other hand, gives a broadening of ≈ 3 meV that typically appears for momentum transfers $\lvert\mathbf{q}\rvert \gtrsim 8\ \mathrm{nm}^{-1}$, i.e., when $\mathbf{q}$ goes outside the first Brillouin zone, thus the same trend as is observed experimentally. This behavior results from the fact that optical phonons are more affected by anharmonicity than acoustic ones. Finally, we note that the increase in linewidth occurs at length and time scales where the differences between ice and water are not so essential. It is likely that the same mechanism or mechanisms cause the broadening in both cases.

I thank F. Sette and G. Ruocco for very useful discussions about their experiment, and M. Altarelli for valuable comments on the manuscript.

[1] F. Sette, G. Ruocco, M. Krisch, U. Bergmann, C. Masciovecchio, V. Mazzacurati, G. Signorelli, and R. Verbeni, Phys. Rev. Lett. **75**, 850 (1995).

[2] G. Ruocco, F. Sette, U. Bergmann, M. Krisch, C. Masciovecchio, V. Mazzacurati, G. Signorelli, and R. Verbeni, Nature **379**, 521 (1996); G. Ruocco, F. Sette, M. Krisch, U. Bergmann, C. Masciovecchio, and R. Verbeni (unpublished).

[3] B. Renker, Phys. Lett. **30A**, 493 (1969).

[4] J. C. Li, D. K. Ross, L. Howe, P. G. Hall, and J. Tomkinson, Physica B **156&157**, 376 (1989).

[5] *Water: A Comprehensive Treatise*, edited by F. Franks (Pergamon, New York, 1972), Vol. 1.

[6] P. V. Hobbs, *Ice Physics* (Clarendon, Oxford, 1974).

[7] W. L. Jorgensen, J. Chandrasekhar, J. D. Madura, R. W. Impey, and M. L. Klein, J. Chem. Phys. **79**, 926 (1983).

[8] J. Bertie and E. Whalley, J. Chem. Phys. **46**, 1271 (1967); P. T. T. Wong and E. Whalley, *ibid.* **65**, 829 (1976).

[9] P. Bosi, R. Tubino, and G. Zerbi, J. Chem. Phys. **59**, 4578 (1973).

[10] J. Li and D. K. Ross, Nature **365**, 327 (1993).

[11] G. Ruocco and F. Sette (private communication).

[12] This result also justifies our neglect of other than nearest-neighbor interactions, whose strength is comparable to the disorder potential.

[13] S. W. Lovesey, *Theory of Neutron Scattering from Condensed Matter* (Clarendon, Oxford, 1984), Vol. 1.

[14] G. D. Mahan, *Many-Particle Physics* (Pergamon, New York, 1990), Chap. 3.